Kovove Mater. 58 2020 395–407
DOI: 10.4149/km_2020_6_395

Microstructure and compressive properties of aluminum matrix syntactic foams containing Al_2O_3 hollow particles

D. W. Rao[1], Y. W. Yang[1], Y. Huang[1], J. B. Sun[1], L. W. Pan[1,2,3]*, Z. L. Hu[1,2,3]

[1] *School of Resources, Environment and Materials, Guangxi University, Nanning 530004, P. R. China*
[2] *Guangxi Key Laboratory of Processing for Non-Ferrous Metals and Featured Materials, Nanning 530004, P. R. China*
[3] *Center Ecological Collaborative Innovation for Aluminum Industry in Guangxi, Nanning 530004, P. R. China*

Received 17 July 2020, received in revised form 4 September 2020, accepted 7 September 2020

Abstract

Al_2O_3 hollow particles were used to manufacture 7055 Al-matrix syntactic foams using a simple gravity infiltration casting method. The effects of infiltration temperature and heat treatment process on microstructures, compressive properties, and energy absorption properties of the prepared Al-matrix syntactic foams were studied. The average density and porosity of the Al-matrix syntactic foams are 1.73 g cm^{-3} and 40.89 %, respectively. The maximum compressive yield strength and compressive strength of the as-cast Al-matrix syntactic foams are 78.23 and 79.52 MPa, respectively. After solution-aging treatment, the compressive strength and yield strength of the Al-matrix syntactic foams are significantly improved. After normalizing, the average compressive plateau stress and energy absorption performance are the best. The highest energy absorption capacity and specific energy absorption are 48.14 MJ m^{-3} and 28.04 kJ kg^{-1}, respectively. This result reached or exceeded the energy absorption properties of many Al-matrix syntactic foams prepared by other processes reported in recent years.

K e y w o r d s: aluminum matrix syntactic foams (AMSFs), gravity infiltration casting, heat treatments, compressive property, energy absorption performance

1. Introduction

Metal matrix syntactic foams (MMSFs) are a class of composite materials consisting of a metal matrix embedded with hollow or porous particles [1]. Compared with polymerized syntactic foams, they have higher compressive yield strength and can be used in higher temperature and worse environments. Like traditional metal foams, MMSFs also have many excellent properties, such as lightweight, high specific strength, high specific stiffness, high energy absorption capability, superior damping, thermal insulation, sound absorption, noise insulation, and electromagnetic shielding. The high energy absorption capacity is the prominent advantage of MMSFs compared to traditional metal foams because of the reinforcement effect of the hollow particles shell. Therefore, they have broad application prospects in the impact-absorbing fields of automobiles, aerospace, military equipment, ships, etc. [2–5]. As energy-absorbing material, the energy absorption properties of MMSFs are affected by the metal matrix, hollow particles, and preparation process.

The types of hollow particles used in metal matrix syntactic foams are fly ash cenospheres [6–8], hollow glass particles [3, 9–12], Al_2O_3 [13–16], SiC [17–21] hollow particles, and expanded pearlite [22, 23]. Fly ash and Al_2O_3 hollow particles are abundant in resources and cheap, so they are more suitable for large-scale industrial applications. At present, the casting method is the way generally used in synthesized MMSFs, especially the infiltration casting method [24]. However, the liquid metal permeability during the infiltration casting process is greatly affected by the size of hollow particles. When the hollow particle size is small (tens of microns), it is necessary to increase the external pressure to enhance the permeability of liquid metal by squeeze casting or gas high-pressure infiltration, which increases process complexity and manufacturing costs. The stirring cast

*Corresponding author: tel.: +86 18776964423; e-mail address: plw988@163.com

Table 1. The nominal composition of the 7055-Al alloy in wt.%

Elements	Si	Fe	Mg	Mn	Cu	Cr	Zn	Ti	Al
Content	0.27	0.46	2.27	0.09	2.38	0.29	8.35	0.20	Bal.

Table 2. Basic parameters of Al_2O_3 hollow particles provided from the manufacturer

Chemical composition (%)				Bulk density ($g\,cm^{-3}$)	Particle size (mm)	Application temperature (℃)
Al_2O_3	Fe_2O_3	SiO_2	Na_2	0.5–1	0.2–5	1800
> 99	≤ 0.15	≤ 0.2	≤ 0.25			

is also the right choice for preparing MMSFs. However, when the hollow microspheres are small, they naturally cluster together, which results in lousy distribution uniformity, especially when the volume fraction of the added hollow microspheres is large, the hollow particle size is small, and the wettability between liquid metal and hollow particles is inferior. Therefore, coarse hollow particles are more suitable for stirring casting. Su et al. [25] successfully prepared syntactic foams composed of aluminum matrices and millimeter Al_2O_3 hollow spheres (1.0–1.5 mm, 1.5–2.0 mm, and 2.0–2.5 mm) by stir casting method. The highest energy absorption capacity of the as-cast AMSFs is 40 $MJ\,m^{-3}$. However, compared with the gravity infiltration casting method, we think the preparation technology of stir casting is sophisticated and the cost increases, and sometimes the shell of hollow microspheres is easily cracked during stirring. For gravity infiltration casting, there is no need for vacuum, gas pressure, mechanical pressure, centrifugal force, and stirring force [16, 26]. The simple process equipment, stable operation, and low cost are conducive to large-scale industrial production. However, the pressure of liquid metal in gravity infiltration casting is limited. Molten metal is difficult to infiltrate into the packed hollow particles with micron size. Therefore, the combination of gravity infiltration casting process and coarse hollow microspheres is a better selection for preparing metal matrix syntactic foams.

Most MMSFs use Al alloys [13, 27–31], Mg alloys [6, 8, 18, 32], Zn alloys [3, 22], Ti alloys [33, 34], and steel [11, 35, 36] as the base material. The compressive strength of syntactic foams is significantly different when using varying metal matrices [24, 37, 38]. In general, the higher the strength and toughness of the metal matrix, the higher the compressive strength of the syntactic foam. Besides, the compressive properties of the syntactic foam prepared by the same metal matrix, but with different heat treatment were also found to be very diverse. AMSFs have been the most widely studied in the last ten years. Among aluminum alloys, 7xxx ultra-high-strength Al alloys (Al-Zn-Mg-Cu) are considered as aviation aluminum that is widely used in aerospace and automotive fields [39]. However, the 7xxx Al alloy matrix syntactic foams have rarely been reported. Balch et al. [37] used 7075 Al alloy and diameters of 15–75 μm ceramic hollow microspheres (composed of alumina and silica Al_2O_3 and SiO_2) to fabricate AMSFs by a custom-built vacuum/pressure infiltrator. The research shows that the compressive strength of the syntactic foam made of 7075 aluminum alloy is twice that of the pure aluminum matrix syntactic foam produced by the same process, and the compressive strength of the peak-aged syntactic foam (T6) was much higher than that of the annealed syntactic foam.

7055 Al alloy is an outstanding representative of the new high strength aluminum alloy. It is an aluminum alloy developed based on increasing the content of Zn and Cu in 7050 aluminum alloy. It not only has a higher strength than 7050 Al alloy but also has strong fracture toughness. In this study, 7055 Al alloy and millimeter-scale Al_2O_3 hollow particles (1–2 mm) are fabricated by gravity infiltration casting. The macro- and microstructure, compressive properties, and energy absorption properties of the syntactic foams were studied under different infiltration temperatures and heat treatments.

2. Experimental

2.1. Materials

The matrix alloy used in this study is in the form of 7055 Al alloy casting rods (ø 20 mm × 200 mm, produced by Southwest Aluminum Group Co., Ltd., China). The chemical composition (shown in Table 1) was determined by Olympus Handheld X-ray Laser Alloy Analyzer – Delta DE2000. The fillers were Al_2O_3 hollow particles provided by Gongyi City Hongle Mineral Products Co., Ltd. (China). Table 2 shows the parameters of the Al_2O_3 hollow particles. A ø 23 mm × 250 mm corundum tube (95 wt.% Al_2O_3) with one

Table 3. Heat treatment processes applied to AMSFs

#	Type of heat treatment	Temperature (℃)	Time (h)	Cooling method	Temperature (℃)	Holding time (h)	Cooling method
1	Normalizing	470	1	Air cooling	–	–	–
2	Annealing	470	1	Furnace cooling	–	–	–
3	Quenching	470	1	Water quenching	–	–	–
4	Solution-aging	470	1	Water quenching	120	24	Air cooling

end welded shut (Yixing Yiming Energy Saving Material Factory, China) was used as the mold for synthesizing syntactic foam. Before the experiment, 1–2 mm diameter Al_2O_3 hollow particles were screened out by using the screen. Some of the Al_2O_3 particles with a break or cracked shells were removed by the gravity sedimentation method. The intact Al_2O_3 hollow particles floated on the water were picked out and cleaned in the alcoholic solution for 5 min by an ultrasonic cleaner. Finally, the washed hollow particles were dried at 200 ℃ for 3 h.

2.2. Gravity infiltration casting process

The necessary steps of synthesizing AMSFs by gravity infiltration casting process are as follows: (1) 60 mm height of Al_2O_3 hollow particles packed beds were filled in a ø 23 mm × 250 mm corundum tube, (2) the corundum tube with hollow particles was fixed vertically in a crucible resistance furnace and preheated at 500 ℃ for 1 h, (2) after preheating, a 7055 Al alloy round bar was placed on the hollow particles in the corundum tube, and the furnace temperature was set at 740, 770, 800, and 830 ℃ to investigate the effect of temperature, (3) when the aluminum alloy bar was melted, a certain amount of covering agent (NaCl : KCl = 1 : 1, wt.%) was added in the melt to prevent evaporation loss of the melt, and (5) the melt infiltrated the gaps among hollow particles by using gravity pressure (pressure of the liquid metal is about 3.8 kPa). The infiltration time was 60 min. After infiltration, the corundum tube was taken out from the furnace and air-cooled. The solidified syntactic foam specimens were demolded and machined for testing.

2.3. Heat treatment process

In this experiment, based on the existing heat treatment process of 7xxx-Al alloy, a variety of heat treatment processes were designed, as shown in Table 3. The heat treatment experiments were carried out in a tube resistance furnace (model SK2-4-12).

2.4. Microstructure and phase analysis

Specimens for microstructural observations were prepared using standard metallographic procedures.

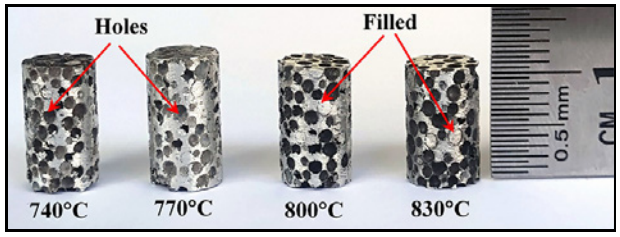

Fig. 1. Macroscopic appearance of AMSFs at different infiltration temperatures.

The detailed process was rough grinding with coarse sandpaper firstly. Secondly, 320, 600, 800, 1000, 1200, 1500, and 2000 mesh water abrasive paper was used for fine grinding. Finally, the finely ground sample was polished on a polishing machine with a polishing paste, and the rotating speed was 900 r min^{-1} so that the sample was evenly pressed on the rotating disc and moved radially from the edge to the center of the disc until a bright mirror surface was obtained. The microstructure was observed by the Phenom ProX scanning electron microscope (SEM). Energy disperse spectroscopy (EDS) was used for composition analysis.

2.5. Quasi-static compression testing

Quasi-static compression tests were conducted on a universal testing machine (WDW3100) at a constant crosshead speed with an initial nominal strain rate of 10^{-3} s^{-1} at ambient temperature. Cylindrical specimens of ø 8 mm × 12 mm were used for uniaxial compression tests. Load and displacement data recorded during the experiment were used to generate the engineering stress-strain curves from which the material properties were calculated.

3. Results and discussion

3.1. As-cast morphology

Figure 1 shows the macromorphology of the samples prepared at different infiltration temperatures. It can be seen that all samples can be thoroughly permeated by liquid metal. Most of the Al_2O_3 hollow

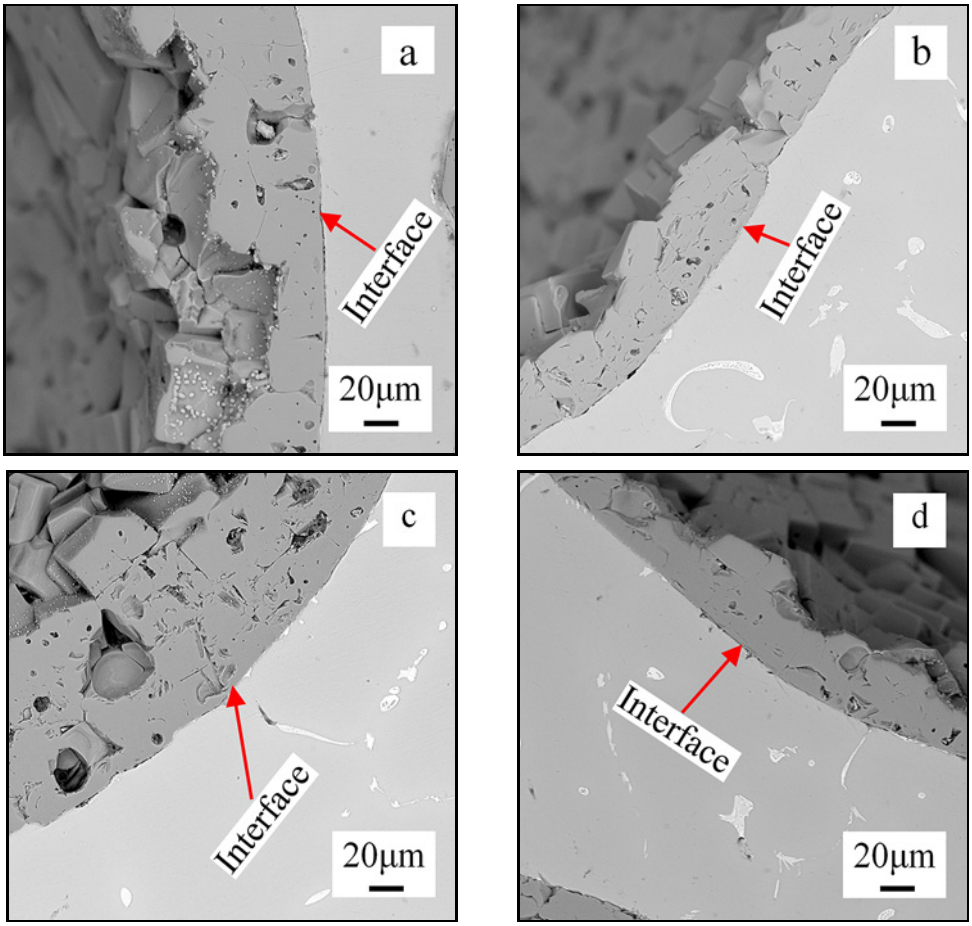

Fig. 2. Interfacial microstructure of syntactic foams under different infiltration temperatures: (a) 740 °C, (b) 770 °C, (c) 800 °C, and (d) 830 °C.

Table 4. EDS analysis results of points in Fig. 4 (at.%)

Position	Al	Zn	Mg	Cu	Fe	Si
A	81.18	–	–	1.12	12.53	5.17
B	34.95	21.90	24.67	18.48	–	–
C	65.80	8.81	14.06	11.33	–	–
D	68.14	8.60	12.28	10.98	–	–
E	64.53	8.84	15.14	11.49	–	–
F	65.37	8.40	16.02	10.21	–	–
G	53.90	13.90	19.93	12.27	–	–

particles in the AMSFs remained intact and were distributed almost evenly. There is no visible gap between the hollow particles and the matrix. However, there are also a few hollow particles filled by the matrix metal, which may be caused by the damage of some thin shell hollow particles that cracked easily in the process of infiltration. Figure 2 shows a typical micrograph of the interface between the aluminum matrix and the Al_2O_3 hollow particle. It can be observed that the interface of samples with different infiltration temperature is clear, continuous, and intact. The interface is tight, and there is no apparent reaction product. In general, the particles and matrix appear to be bonded well at all infiltration temperatures. Usually, the aluminum liquid is incompatible with alumina ceramics, so it is difficult to wet alumina ceramics. However, good interface bonding has been achieved in this experiment. We think this situation is related to the existence of the Mg element in the 7055 Al alloy matrix. It has been reported in the literature [40–42] that adding Mg to aluminum alloy can improve the wettability of aluminum liquid and alumina.

Figure 3 shows the as-cast microstructure of the syntactic foams matrix at different infiltration tempe-

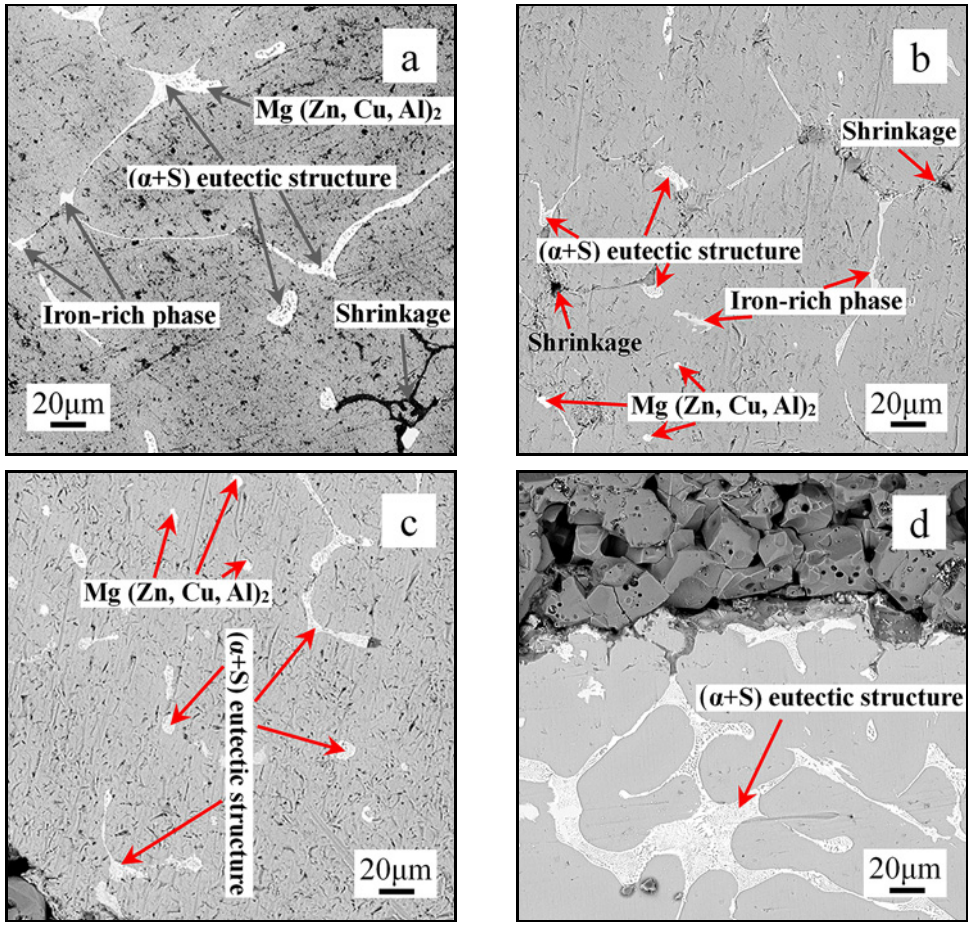

Fig. 3. Microstructure of as-cast AMSFs matrix at different infiltration temperatures: (a) 740 ℃, (b) 770 ℃, (c) 800 ℃, and (d) 830 ℃.

ratures. The white, gray, and dark gray second phase precipitates are shown in the matrix. The research results of Xu [43] and Wen [44] showed that the precipitates of as-cast Al-Zn-Mg-Cu alloy are mainly composed of $Mg(Zn,Cu,Al)_2$-, $S(Al_2CuMg)$-, $\theta(Al_2Cu)$-, and iron-rich-phases. The primary precipitates in the syntactic foam matrix were analyzed by EDS (Fig. 4, Table 4). The independent, bright white lumps were $Mg(Zn,Cu,Al)_2$-phases. The EDS detected the iron element in the gray phase, which indicates that it was the iron-rich phase. Similarly, EDS spot scanning analysis was carried out for the reticular structure formed by the white phase and dark gray phase. The white phase is $S(Al_2CuMg)$-phase [44], and the dark gray phase is the α-Al-phase, so the structure is (α + S) eutectic structure. It can be seen from Fig. 3 that the precipitated structure at 740 ℃ is (α + S) eutectic structure accompanied by a small amount of $Mg(Zn,Cu,Al)_2$-phase, and there are many long iron-rich phases precipitated. At 770 and 800 ℃, the (α + S) eutectic structure decreased, and there was more granular $Mg(Zn,Cu,Al)_2$-phase distribution. Also, no iron-rich phase was detected at 800 ℃. However, there were still longer iron-rich phases at 770 ℃. When

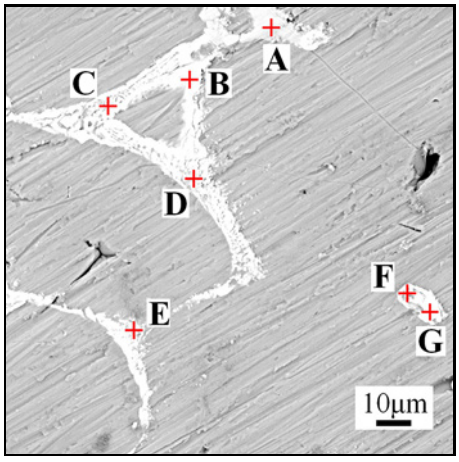

Fig. 4. EDS analysis area of the syntactic foam matrix phase.

the infiltration temperature increased to 830 ℃, the amount of (α + S) eutectic structure increased, and the size became coarse.

Besides, some black void areas can be observed at 740 and 770 ℃, which is considered to be the inter-

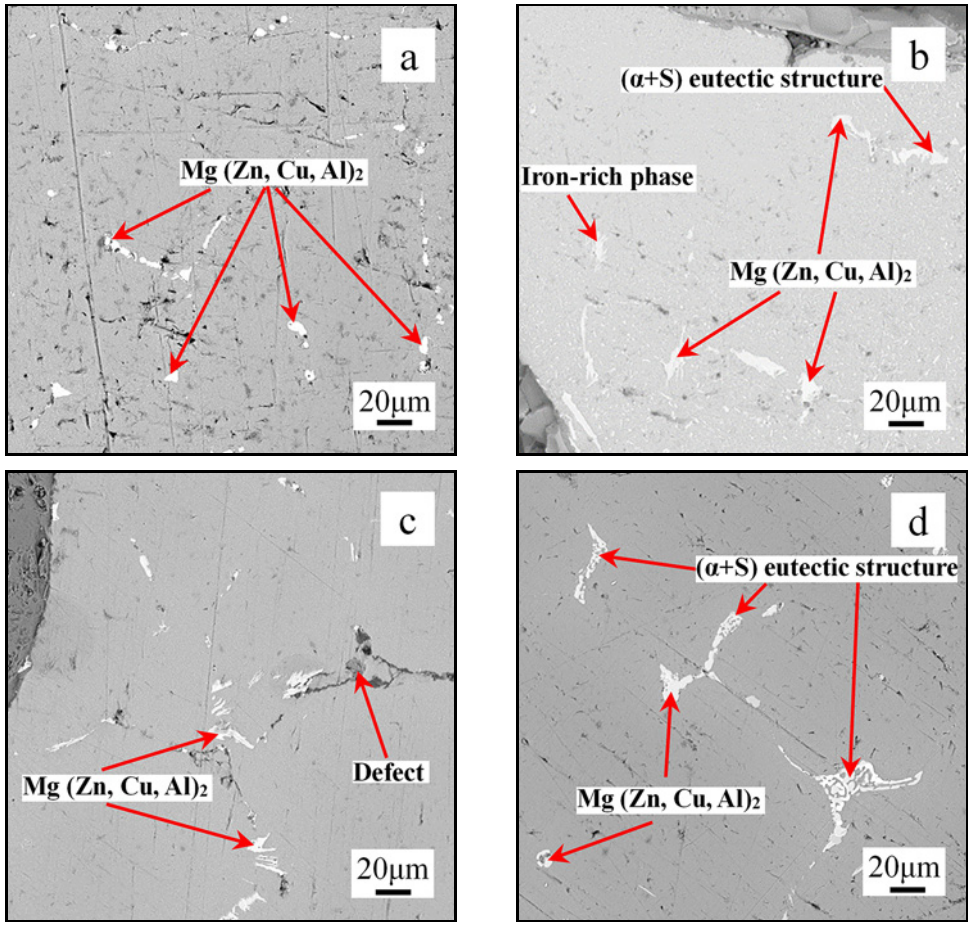

Fig. 5. Microstructure of AMSFs with different heat treatment processes: (a) normalizing: 470 °C/1 h/AC, (b) annealing: 470 °C/1 h/FC, (c) quenching: 470 °C/1 h/WQ, and (d) solution-aging: 470 °C/1 h/WQ + 120 °C/24 h/AC.

dendritic shrinkage caused by inadequate local feeding of liquid metal. Although the temperature was far higher than the liquidus of aluminum alloy, and the molten aluminum had good fluidity, the infiltration of aluminum liquid into the narrow and curved hollow particles gaps was not conducive to timely feeding, so there would be local micro shrinkage. However, when the infiltration temperature was increased to 800 and 830 °C, no micro shrinkage was observed in the matrix, which indicates that the increase of infiltration temperature is conducive to reduce the micro shrinkage defects in the matrix.

3.2. Heat treatment effect on the syntactic foam microstructure

The syntactic foam samples infiltrated at 800 °C were heat-treated using different processes. These processes included normalizing, annealing, quenching, and solution-aging, as shown in Table 3. The microstructures of heat-treated samples are shown in Fig. 5. From the macroscopic structure, there is no apparent difference between the heat-treated sample and the as-cast sample, which indicates that the heat treatment does not affect the pore structure (size and distribution) of the syntactic foams.

It can be observed from Fig. 5 that the microstructures of the syntactic foams changed considerably after heat treatment. After normalizing, no (α + S) eutectic structure was found in the matrix, and there were many bright white Mg(Zn,Cu,Al)$_2$-phases precipitated and distributed evenly. After annealing, there were many coarse Mg(Zn,Cu,Al)$_2$-phases precipitated, and a small number of iron-rich-phases precipitated. After quenching, there were apparent defects in the matrix, and there were bright white short bar massive phases precipitated near the crack. The matrix microstructure of the syntactic foams after solution-aging treatments was (α + S) eutectic structure accompanied by Mg(Zn,Cu,Al)$_2$-phases.

3.3. Density and porosity content

The density of the matrix alloy is 2.81 g cm^{-3}. The density of the syntactic foam is calculated by measuring the volume and quality of the syntactic foam. The results are shown in Table 5. The Al_2O_3 hollow particles used in this study were almost spherical, but

Table 5. Density and porosity of syntactic foams

Samples condition	Processing parameter	Density ($g\,cm^{-3}$)	Porosity (%)
As-cast	7055-Al alloy	2.81	0
	Syntactic foam, infiltration at 740 ℃	1.75	40.23
	Syntactic foam, infiltration at 770 ℃	1.73	40.98
	Syntactic foam, infiltration at 800 ℃	1.74	40.61
	Syntactic foam, infiltration at 830 ℃	1.77	39.46
Heat treatment	Syntactic foam, normalizing, 470 ℃/1 h/AC	1.72	41.36
	Syntactic foam, annealing, 470 ℃/1 h/FC	1.76	39.85
	Syntactic foam, quenching, 470 ℃/1 h/WQ	1.61	45.54
	Syntactic foam, solution-aging, 470 ℃/1 h/WQ + 120 ℃/24 h/AC	1.78	39.10
	Average value (syntactic foams)	1.73	40.89

the shape of the inner and outer walls of the spherical shell shows certain asymmetry. Therefore, the wall thickness may be different for each Al_2O_3 hollow particles. For these reasons, it may be difficult to quantify the ratio of wall thickness (t) to diameter (D) [45]. By considering the geometry of the sphere and the average density of the sphere, one method to determine the t/D ratio is derived, as shown in Eq. (1) [45]:

$$\rho_{HP} = \rho_{Al_2O_3} \frac{\frac{4}{3}\pi\frac{D^3}{8} - \frac{4}{3}\pi\frac{d^3}{8}}{\frac{4}{3}\pi\frac{D^3}{8}} = \rho_{Al_2O_3}\left(1 - \frac{d^3}{D^3}\right), \tag{1}$$

where ρ_{HP} is the density of Al_2O_3 hollow particle, and d is the internal diameter of the Al_2O_3 hollow particle. The t/D ratio of hollow particles can be determined by Eq. (2) from the density of Al_2O_3 and hollow particle [45]:

$$\frac{t}{D} = \frac{1}{2}\left[1 - \left(1 - \frac{\rho_{HP}}{\rho_{Al_2O_3}}\right)^{\frac{1}{3}}\right]. \tag{2}$$

The ratio of the inner radius (r_i) to the outer radius (r_o) of the hollow particle is defined as the radius ratio ($\eta = r_i/r_o$). The relationship between the radius ratio and the wall thickness of the hollow particle is Eq. (3) [45, 46]:

$$t = r_o(1 - \eta). \tag{3}$$

The volume fraction of porosity in hollow particles, Φ_{HP}, can be estimated as Eq. (4) [45, 46]:

$$\Phi_{HP} = \eta^3. \tag{4}$$

The hollow particles volume fraction and porosity of AMSFs were calculated using rule-of-mixture (ROM) [9, 46]:

$$\rho_{sf} = \rho_m(1 - V_{HP}) + \rho_{HP}V_{HP}, \tag{5}$$

$$\Phi_v = \Phi_{HP}V_{HP}, \tag{6}$$

where ρ_{sf} is the density of the syntactic foam, ρ_m is the density of 7055 alloy matrix, ρ_{HP} is the average density of hollow particles, Φ_{HP} is the porosity in a hollow particle, V_{HP} is the hollow particle volume fraction in syntactic foam, and Φ_v is the porosity of the syntactic foam. As a result, the hollow particle volume fraction was 52 %. In Table 5, it is observed that it is slightly different under different conditions, which indicates that the distribution of Al_2O_3 hollow particles is uniform in each sample. The average density of the syntactic foam is 1.73 $g\,cm^{-3}$, which is 38.4 % lower than that of the 7055 Al alloy matrix. The average density is similar to that of 7075 aluminum alloy matrix syntactic foams researched by Balch using gas pressure infiltration casting [37]. The average porosity of all syntactic foam samples was 40.89 %. The fluctuation of porosity is mainly due to the small number of hollow particles filled by liquid.

3.4. Compressive behavior

3.4.1. Compressive deformation behavior

Figure 6 shows the stress-strain curves for as-cast and heat treatment syntactic foams tested under quasi-static compression. It can be seen that the compression curve shapes of matrix alloy and syntactic foams material are quite different. The compression curve of matrix alloy rises sharply due to the strain hardening effect after the yield point. For the syntactic foams, there are three distinct regions in the stress-strain curve: An initial linear elastic stage before reaching the peak strength (I), followed by the platform stage with unchanged stress and a more prolonged strain (II), and the final densification stage that starts at strain approximately 70–75 % (III). These characteristics are similar to those of most metal foams and MMSFs [3, 27, 47–50]. Generally speak-

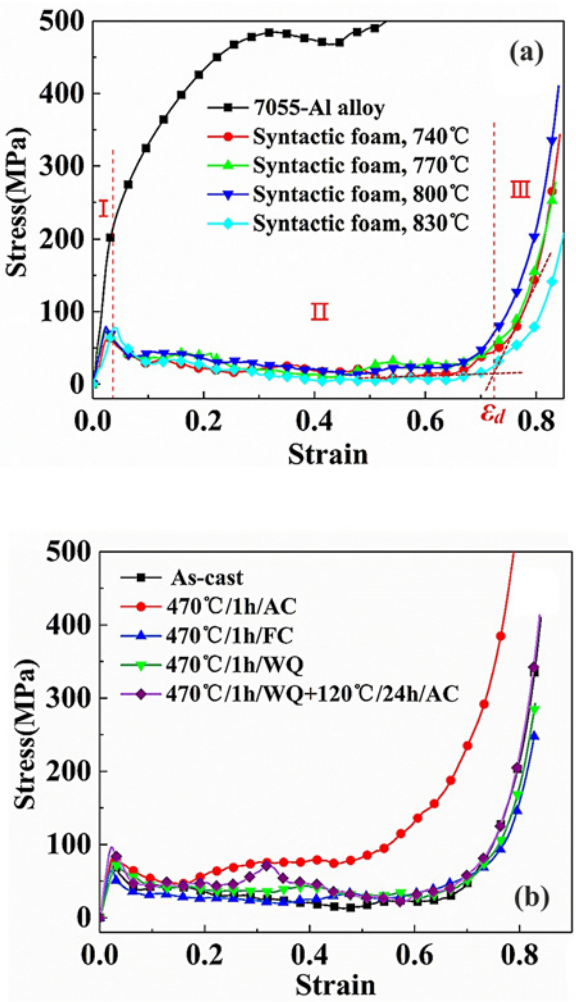

Fig. 6. Compressive stress-strain curves for (a) as-cast syntactic foams at different infiltration temperature and (b) syntactic foams subjected to different heat treatments.

ing, there is a distinct peak in the transition from I to II, which can be called the compressive strength of the syntactic foams. Before the peak stress, the external load is supported by the metal matrix framework and the Al_2O_3 hollow particles shells. With the increase of pressure and strain, part of the hollow particles starts to be elastically bent. When the elastic limit is almost reached, some hollow particles begin to collapse and break (because the elastic limit strain of hollow particles is smaller than that of the matrix). The hollow particles shells lose their bearing capacity and make the compression stress drop rapidly. At this point, the syntactic foams matrix is still bearing the load, and strain hardening of the matrix is also continuing. However, due to the small bearing area of the cross-section of the specimen, the matrix cannot bear the external load independently, and the hollow particles mainly carry the load. With the increase of strain, a batch by batch of hollow particles were continuously bent, collapsed, and crushed, which leads to the wave-like fluctuation of stress. The volume fraction of hollow particles in the sample is large, so there is a longer compression yield platform. When all the hollow particles are completely crushed, the stress starts to rise again. At this time, the load is jointly supported by the matrix and the crushed hollow particle shells. Both of them suffer strain hardening, so the stress rising stage of densification and compaction appears. The whole compression yield platform is mainly the bending, collapse, and crushing process of hollow particles. During this process, a large number of hollow particles are crushed, and a lot of energy is absorbed, and thus the syntactic foams show the characteristics of energy absorption buffering.

3.4.2. Compressive properties

The quasi-static compressive properties of syntactic foams under different conditions are presented in Table 6. It includes yield strength ($\sigma_y = \sigma_{0.2\%}$), compressive strength, average plateau stress σ_{pl}, and densification strain ε_d [45, 51]. The compressive properties of as-cast samples increased and then decreased with

Table 6. Compressive properties of syntactic foams at different conditions

Condition	Process parameters	σ_y (MPa)	Compressive strength (MPa)	σ_{pl} (MPa)	ε_d (%)
As-cast	Infiltration at 740 ℃	61.46	65.18	19.51	70.58
As-cast	Infiltration at 770 ℃	74.74	75.45	25.94	70.41
	Infiltration at 800 ℃	78.23	79.52	26.60	69.83
	Infiltration at 830 ℃	77.47	77.74	13.62	72.88
Heat treatment	Normalizing, 470 ℃/1 h/AC	83.28	84.54	78.63	63.16
	Annealing, 470 ℃/1 h/FC	63.19	64.58	28.87	67.91
	Quenching, 470 ℃/1 h/WQ	68.53	71.53	37.97	71.74
	Solution-aging, 470 ℃/1 h/WQ + 120 ℃/24 h/AC	95.32	96.45	43.43	72.46

the increase of infiltration temperature. When the infiltration temperature was 800 ℃, the highest values of yield strength, compressive strength, and plateau stress were 78.23, 79.52, and 26.6 MPa, respectively. This result is closely related to the microstructure of the matrix. The S(Al_2CuMg)-phase in the eutectic structure of (α + S) is a brittle phase [43, 44, 52]. At 800 ℃, the amount of S(Al_2CuMg)-phase is less, and the size of the eutectic group is small. $Mg(Zn,Cu,Al)_2$ particles are distributed uniformly, which is beneficial to improve the compression properties. Besides, the number of long iron-rich-phases decreased obviously at 800 ℃, while there were many long iron-rich phases at 740 and 770 ℃. The coarse (α + S) eutectic structure at 830 ℃ was not conducive to the improvement of compressive properties. It should be noted that the micro shrinkage of the matrix caused by insufficient feeding at 740 and 770 ℃ may also be one of the reasons for the low compression performance. The different infiltration temperature had little effect on the densification strain of the syntactic foams, and it remained at 70 % or so.

After heat treatment, the compressive properties of the syntactic foams increased, and some of them decreased. Normalizing and solution-aging significantly increased the yield strength and compressive strength of the syntactic foams. But annealing and quenching reduced the yield strength and compressive strength, while the average plateau stress after heat treatment all had been significantly improved. The yield strength of the syntactic foam after solution--aging is 95.32 MPa, and the compressive strength is 96.45 MPa. The average plateau stress of the sample is 78.63 MPa after normalizing. After normalizing, no (α + S) eutectic structure was observed in the matrix. There were many bright white $Mg(Zn,Cu,Al)_2$--phases precipitated and distributed uniformly, which was beneficial to the improvement of compressive properties. Besides, due to the mismatch of the thermal expansion coefficient between the metal matrix and the Al_2O_3 ceramic particles, there is always residual compressive stress at the syntactic foam interface after solidification [3]. Normalizing releases the residual compressive stress between the matrix and the hollow particles, which is also an essential factor to improve compression performance [3]. After solution--aging, the (α + S) eutectic structure in the matrix is reduced, and bright white $Mg(Zn,Cu,Al)_2$-phases precipitate out, which is conducive to improving the compressive properties. Because of the deterioration of the matrix structure and properties of the hollow particles by annealing and quenching, their overall compressive properties are relatively low.

Also, the average plateau stress of the syntactic foams after heat treatment has been improved notably. We think that heat treatment may have the effect of enhancing the strength of Al_2O_3 hollow particle shells. The yield strength and compressive strength of the syntactic foams mainly depend on the strength of the matrix and the hollow particle shells, and they share the external load before the peak stress. After the peak stress (compression yield platform), the external load is mainly supported by the hollow particles. Thus the increase of compression plateau stress should be related to the strength increase of hollow particles, and that also shows the strength of the hollow particle shells has an essential effect on the compressive properties of syntactic foams. The strengthening effect of particle shells in MMSFs makes them attain higher compression plateau stress than in traditional metal foams. For conventional aluminum foams, there is no enhancement effect of hollow particle shells, coupled with their relatively high porosity (80–95 %); generally, the compression plateau stress of traditional aluminum foams is lower, and their energy absorption capacity is usually less than 10 MJ m^{-3} [53–55].

3.4.3. Energy absorption properties

During the compression deformation, the energy absorbed by syntactic foams is an important index. Generally, the energy absorption capacity is determined by calculating the area of the compressive stress-strain curve up to densification strain (ε_d) by [3]:

$$W = \int_0^{\varepsilon_d} \sigma(\varepsilon) d\varepsilon, \tag{7}$$

where W has units corresponding to the energy per unit volume of the material (MJ m^{-3}). The energy absorption efficiency is defined as the ratio of the energy absorbed by a material in the actual compression process to that absorbed by an ideal compression process under arbitrary strain. It is calculated by [23, 56]:

$$\xi = \frac{A_{real}}{A_{ideal}} = \frac{\int_0^{\varepsilon_d} \sigma(\varepsilon) d\varepsilon}{\sigma_{max}\varepsilon_d}, \tag{8}$$

where σ_{max} is the highest compressive stress up to ε_d. Also, the specific energy absorption (E_s) is the energy absorption capacity divided by the foam density [3, 27]:

$$E_s = \frac{W_{\varepsilon_d}}{\rho_{sf}}, \tag{9}$$

where W_{ε_d} is the energy absorption capacity of the material and ρ_{sf} is the density of AMSFs. The energy absorption properties of AMSFs after casting and heat treatment are given in Table 7. It can be seen that the change in energy absorption performance is similar to the compression performance shown in Table 6. For the as-cast syntactic foam, the maximum energy

Table 7. Energy absorption properties of 7055Al-matrix syntactic foams at different conditions

Condition	Process parameters	ε_d (%)	W_{ε_d} (MJ m^{-3})	E_s (kJ kg^{-1})	ξ (%)
As-cast	Infiltration at 740 ℃	70.58	15.93	9.15	56.52
	Infiltration at 770 ℃	70.41	20.34	11.75	69.74
	Infiltration at 800 ℃	69.83	20.58	11.84	67.97
	Infiltration at 830 ℃	72.88	12.95	7.38	64.33
Heat treatment	Normalizing, 470 ℃/1 h/AC	63.16	48.14	28.04	50.64
	Annealing, 470 ℃/1 h/FC	67.91	20.67	11.73	61.28
	Quenching, 470 ℃/1 h/WQ	71.74	27.93	17.39	65.01
	Solution-aging, 470 ℃/1 h/WQ + 120 ℃/24 h/AC	72.46	32.84	18.45	59.94

Table 8. Comparison of compressive energy absorption capacity of syntactic foams from the present work with AMSFs reported in recent years

Preparation method	AMSFs	ρ (g cm^{-3})	W_{ε_d} (MJ m^{-3})	E_s (kJ kg^{-1})	Ref.	Year
Gravity infiltration	7055 Al alloy	1.73	48.14	28.04	Present work	2020
Microwave sintering	Pure Al	1.85	18.61	8.09	[57]	2019
Stirring casting	ZL111 Al alloy	2.05	47.31	23.08	[25]	2019
Stirring casting	AA2014 Al alloy	1.99	65	32.66	[58]	2019
Counter-gravity infiltration	A356 Al alloy	1.06–1.11	19.8	17.8–18.7	[23]	2018
Pressure infiltration	5A03 Al alloy	1.22	51.2	42.0	[9]	2018
Pressure infiltration	A356 Al alloy	0.76	6.6	8.68	[27]	2017
Pressure infiltration	Pure Al	1.20	35.7	29.8	[12]	2017
Pressure infiltration	5A03 Al alloy	1.23	60.8	49.4	[12]	2017
Pressure infiltration	5A06 Al alloy	1.40	62.8	44.9	[12]	2017
Stirring casting	AA2014 alloy	2.11	23.5	11.15	[59]	2017
Vacuum casting	Al-12Si alloy	1.13	7	6.2	[60]	2017
Squeeze casting	Pure Al	2.20	15.42	7	[61]	2016
Pressure infiltration	A356 Al alloy	2.32	55.19	23.78	[62]	2016
Pressure infiltration	A356 Al alloy	1.07	26.5	24.8	[2]	2015
Powder metallurgy	Pure Al	2.36	34.88	14.8	[46]	2015
Pressure infiltration	A380 Al alloy	1.86	57.7	31	[63]	2014
Gravity infiltration	A355.0 Al alloy	1.20	18	15	[64]	2014
Pressure infiltration	A206 Al alloy	1.93	63.2	32.75	[17]	2013
Pressure infiltration	6082 Al alloy	1.24	30.9	25	[48]	2009
Squeeze casting	Pure Al	1.43	20–35	14–23	[49]	2007

absorption and specific energy absorption of the syntactic foam reached 20.58 MJ m^{-3} and 11.84 kJ kg^{-1} at 800 ℃, respectively. The syntactic foams after heat treatment have better energy absorption capacity and specific energy absorption, after normalizing, reaching 48.14 MJ m^{-3} and 28.04 kJ kg^{-1}, respectively. The relationship between energy absorption capacity and compression strain is shown in Fig. 7. It can be seen that the relationship curves are all almost linear. The curves have no mutation, which indicates the compression platform is relatively stable, and these syntactic foams are more suitable for energy absorption materials. It can be observed from Table 8 that the results of this study reach or exceed the energy absorption properties of some AMSFs fabricated by pressure infiltration casting, squeeze casting, and stir casting in recent years, which indicates the simple process and the cheap Al_2O_3 hollow particles applied in this study have a potential advantage in large-scale industrial production.

4. Conclusions

1. The 7055 Al alloy melt has excellent seepage behavior and interfacial bonding with hollow particles at 740, 770, 800, and 830 ℃. With the increase of infiltration temperature, the eutectic structure of matrix (α + S) decreases, and there is granular $Mg(Zn,Cu,Al)_2$-phase distribution. When the temperature is 830 ℃, the eutectic structure of (α + S) increases, and the size becomes coarse.

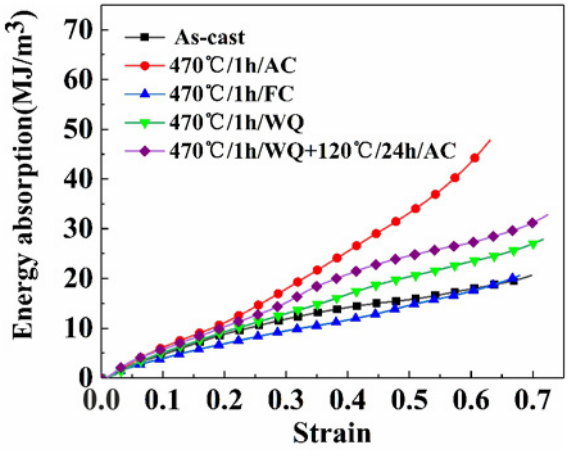

Fig. 7. The curvilinear relationship between energy absorption capacity and compressive strain in syntactic foams under different conditions.

2. The average density and porosity of the AMSFs are 1.73 g cm^{-3} and 40.9 %, respectively. When the infiltration temperature is 800 ℃, the compressive properties of as-cast syntactic foams are the best. The yield strength, compressive strength, and the average plateau stress are 78.23, 79.52, and 26.6 MPa, respectively. After normalizing, the average plateau stress is significantly improved, reaching 78.63 MPa. Solution-aging has a significant effect on enhancing yield strength and compressive strength. The maximum yield strength is 95.32 MPa, and the compressive strength is 96.45 MPa.

3. Normalizing increased the energy absorbing capacity and specific energy absorption of the as-cast syntactic foams. The maximum energy absorption capacity of the heat-treated syntactic foam was 48.14 MJ m^{-3}, and the specific energy absorption was 28.04 kJ kg^{-1}, which reaches or exceeds many AMSFs prepared by gas pressure infiltration casting, squeeze casting, and stir casting in recent years.

Acknowledgements

The authors acknowledge the Youth Fund of Guangxi Key Laboratory of Processing for Non-ferrous Metal and Featured Materials (GXYSYF1806), Guangxi Natural Science Foundation (Grant No. 2016GXNSFAA380223), Guangxi University Research Fund Project (Grant No. XJZ100343), Innovation Drive Development Foundation of Guangxi (Grant No. AA17202011), Innovation and Entrepreneurship Training Program for College Students of Guangxi University (201810593230). Jieming Wen is thanked for providing the electronic universal testing machine for the compression test.

References

[1] Y. Zhao, X. Tao, X. Xue, Manufacture and mechanical properties of metal matrix syntactic foams, Materials Science & Technology Conference and Exhibition (MS&T'08), Volume 4 (2008) pp. 2607–2615. ISBN 978-160560621-7.

[2] M. Taherishargh, I. V. Belova, G. E. Murch, T. Fiedler, Pumice/aluminium syntactic foam, Mater. Sci. Eng. A 635 (2015) 102–108. doi:10.1016/j.msea.2015.03.061

[3] L. Pan, Y. Yang, M. U. Ahsan, D. D. Luong, N. Gupta, A. Kumar, P. K. Rohatgi, Zn-matrix syntactic foams: Effect of heat treatment on microstructure and compressive properties, Mater. Sci. Eng. A 731 (2018) 413–422. doi:10.1016/j.msea.2018.06.072

[4] M. Garcia-Avila, M. Portanova, A. Rabiei, Ballistic performance of a composite metal foam-ceramic armor system, Procedia Mater. Sci. 4 (2014) 145–150. doi:10.1016/j.mspro.2014.07.571

[5] M. Goel, V. Matsagar, A. Gupta, Blast resistance of stiffened sandwich panels with aluminum cenosphere syntactic foam, Int. J. Impact Eng. 77 (2015) 134–146. doi:10.1016/j.ijimpeng.2014.11.017

[6] K. N. Braszczyńska-Malik, J. Kamieniak, AZ91 magnesium matrix foam composites with fly ash cenospheres fabricated by negative pressure infiltration technique, Mater. Charact. 128 (2017) 209–216. doi:10.1016/j.matchar.2017.04.005

[7] K. N. Braszczyńska-Malik, J. Kamieniak, Analysis of interface between components in AZ91 magnesium alloy foam composite with Ni-P coated fly ash cenospheres, J. Alloys Compd. 720 (2017) 352–359. doi:10.1016/j.jallcom.2017.05.285

[8] V. Manakari, G. Parande, M. Gupta, Effects of hollow fly-ash particles on the properties of magnesium matrix syntactic foams: A review, Mater. Perform. Charact. 5 (2016) 116–131. doi:10.1520/MPC20150060

[9] Q. Zhang, Y. Lin, H. Chi, J. Chang, G. Wu, Quasi-static and dynamic compression behavior of glass cenospheres/5A03 syntactic foam and its sandwich structure, Compos. Struct. 183 (2018) 499–509. doi:10.1016/j.compstruct.2017.05.024

[10] G. Anbuchezhiyan, B. Mohan, D. Sathianarayanan, T. Muthuramalingam, Synthesis and characterization of hollow glass microspheres reinforced magnesium alloy matrix syntactic foam, J. Alloys Compd. 719 (2017) 125–132. doi:10.1016/j.jallcom.2017.05.153

[11] D. D. Luong, V. C. Shunmugasamy, N. Gupta, D. Lehmhus, J. Weise, J. Baumeister, Quasi-static and high strain rates compressive response of iron and Invar matrix syntactic foams, Mater. Des. 66 (2015) 516–531. doi:10.1016/j.matdes.2014.07.030

[12] Y. Lin, Q. Zhang, F. Zhang, J. Chang, G. Wu, Microstructure and strength correlation of pure Al and Al-Mg syntactic foam composites subject to uniaxial compression, Mater. Sci. Eng. A 696 (2017) 236–247. doi:10.1016/j.msea.2017.04.060

[13] D. P. Mondal, M. D. Goel, V. Upadhyay, S. Das, M. Singh, A. K. Barnwal, Comparative study on microstructural characteristics and compression deformation behaviour of alumina and cenosphere reinforced aluminum syntactic foam made through stir casting technique, Trans. Indian Inst. Met. 71 (2018) 567–577. doi:10.1007/s12666-017-1211-x

[14] M. Y. Omar, C. Xiang, N. Gupta, O. M. Strbik, K. Cho, Syntactic foam core metal matrix sandwich composite under bending conditions, Mater. Des. 86 (2015) 536–544. doi:10.1016/j.matdes.2015.07.127
[15] H. Lin, H. Y. Wang, C. Lu, L. H. Dai, A metallic glass syntactic foam with enhanced energy absorption performance, Scr. Mater. 119 (2016) 47–50. doi:10.1016/j.scriptamat.2016.03.034
[16] G. Castro, S. R. Nutt, Synthesis of syntactic steel foam using gravity-fed infiltration, Mater. Sci. Eng. A 553 (2012) 89–95. doi:10.1016/j.msea.2012.05.097
[17] G. A. Rocha Rivero, B. F. Schultz, J. B. Ferguson, N. Gupta, P. K. Rohatgi, Compressive properties of Al-A206/SiC and Mg-AZ91/SiC syntactic foams, J. Mater. Res. 28 (2013) 2426–2435. doi:10.1557/jmr.2013.176
[18] H. Anantharaman, V. C. Shunmugasamy, O. M. Strbik, N. Gupta, K. Cho, Dynamic properties of silicon carbide hollow particle filled magnesium alloy (AZ91D) matrix syntactic foams, Int. J. Impact Eng. 82 (2015) 14–24. doi:10.1016/j.ijimpeng.2015.04.008
[19] J. Cox, D. Luong, V. C. Shunmugasamy, N. Gupta, O. Strbik, K. Cho, Dynamic and thermal properties of aluminum alloy A356/silicon carbide hollow particle syntactic foams, Metals 4 (2014) 530–548. doi:10.3390/met4040530
[20] D. P. Mondal, M. D. Goel, N. Bagde, N. Jha, S. Sahu, A. K. Barnwal, Closed cell ZA27-SiC foam made through stir-casting technique, Mater. Des. 57 (2014) 315–324. doi:10.1016/j.matdes.2013.12.026
[21] S. Sahu, D. P. Mondal, J. U. Cho, M. D. Goel, M. Z. Ansari, Low-velocity impact characteristics of closed cell AA2014-SiCp composite foam, Composites, Part B 160 (2019) 394–401. doi:10.1016/j.compositesb.2018.12.054
[22] S. Broxtermann, M. Vesenjak, L. Krstulović-Opara, T. Fiedler, Quasi static and dynamic compression of zinc syntactic foams, J. Alloys Compd. 768 (2018) 962–969. doi:10.1016/j.jallcom.2018.07.215
[23] M. Taherishargh, E. Linul, S. Broxtermann, T. Fiedler, The mechanical properties of expanded perlite-aluminium syntactic foam at elevated temperatures, J. Alloys Compd. 737 (2018) 590–596. doi:10.1016/j.jallcom.2017.12.083
[24] Y. Zhao, X. Tao, Behaviour of metal matrix syntactic foams in compression, Materials Science & Technology Conference and Exhibition (MS&T'09) (2009) pp. 1785–1793. ISBN 978-1-61567-636-1.
[25] M. Su, H. Wang, H. Hao, Compressive properties of aluminum matrix syntactic foams prepared by stir casting method, Adv. Eng. Mater. 21 (2019) 1900183. doi:10.1002/adem.201900183
[26] L. Pan, D. Rao, Y. Yang, J. Qiu, J. Sun, N. Gupta, Z. Hu, Gravity casting of aluminum-Al_2O_3 hollow sphere syntactic foams for improved compressive properties, J. Porous Mater. 27 (2020) 1127–1137. doi:10.1007/s10934-020-00889-x
[27] S. Broxtermann, M. Taherishargh, I. V. Belova, G. E. Murch, T. Fiedler, On the compressive behaviour of high porosity expanded Perlite-Metal Syntactic Foam (P-MSF), J. Alloys Compd. 691 (2017) 690–697. doi:10.1016/j.jallcom.2016.08.284
[28] B. Katona, A. Szlancsik, T. Tábi, I. N. Orbulov, Compressive characteristics and low frequency damping of aluminium matrix syntactic foams, Mater. Sci. Eng. A 739 (2019) 140–148. doi:10.1016/j.msea.2018.10.014
[29] J. Maria, B. Schultz, J. B. Ferguson, P. Rohatgi, Al-Al_2O_3 syntactic foams – Part I: Effect of matrix strength and hollow sphere size on the quasi-static properties of Al-A206/Al_2O_3 syntactic foams, Mater. Sci. Eng. A 582 (2013) 415–422. doi:10.1016/j.msea.2013.05.081
[30] L. P. Zhang, Y. Y. Zhao, Mechanical response of Al matrix syntactic foams produced by pressure infiltration casting, J. Compos. Mater. 41 (2007) 2105–2117. doi:10.1177/0021998307074132
[31] T. Fiedler, K. Al-Sahlani, P. A. Linul, E. Linul, Mechanical properties of A356 and ZA27 metallic syntactic foams at cryogenic temperature, J. Alloys Compd. 813 (2020) 152181. doi:10.1016/j.jallcom.2019.152181
[32] A. Daoud, M. T. Abou El-khair, M. Abdel-Aziz, P. Rohatgi, Fabrication, microstructure and compressive behavior of ZC63 Mg-microballoon foam composites, Compos. Sci. Technol. 67 (2007) 1842–1853. doi:10.1016/j.compscitech.2006.10.023
[33] D. P. Mondal, J. Datta Majumder, N. Jha, A. Badkul, S. Das, A. Patel, G. Gupta, Titanium-cenosphere syntactic foam made through powder metallurgy route, Mater. Des. 34 (2012) 82–89. doi:10.1016/j.matdes.2011.07.055
[34] N. Jha, D. P. Mondal, M. D. Goel, J. D. Majumdar, S. Das, O. P. Modi, Titanium cenosphere syntactic foam with coarser cenosphere fabricated by powder metallurgy at lower compaction load, Trans. Nonferrous Met. Soc. China 24 (2014) 89–99. doi:10.1016/S1003-6326(14)63032-6
[35] L. Peroni, M. Scapin, C. Fichera, D. Lehmhus, J. Weise, J. Baumeister, M. Avalle, Investigation of the mechanical behaviour of AISI 316L stainless steel syntactic foams at different strain-rates, Composites, Part B 66 (2014) 430–442. doi:10.1016/j.compositesb.2014.06.001
[36] J. Weise, N. Salk, U. Jehring, J. Baumeister, D. Lehmhus, M. A. Bayoumi, Influence of powder size on production parameters and properties of syntactic Invar foams produced by means of metal powder injection moulding, Adv. Eng. Mater. 15 (2013) 118–122. doi:10.1002/adem.201200129
[37] D. K. Balch, J. G. O'Dwyer, G. R. Davis, C. M. Cady, G. T. Gray, D. C. Dunand, Plasticity and damage in aluminum syntactic foams deformed under dynamic and quasi-static conditions, Mater. Sci. Eng. A 391 (2005) 408–417. doi:10.1016/j.msea.2004.09.012
[38] R. A. Palmer, K. Gao, T. M. Doan, L. Green, G. Cavallaro, Pressure infiltrated syntactic foams – Process development and mechanical properties, Mater. Sci. Eng. A 464 (2007) 85–92. doi:10.1016/j.msea.2007.01.116
[39] J. Shin, T. Kim, D. Kim, D. Kim, K. Kim, Castability and mechanical properties of new 7xxx aluminum alloys for automotive chassis/body applications, J. Alloys Compd. 698 (2017) 577–590. doi:10.1016/j.jallcom.2016.12.269
[40] A. Bahrami, M. I. Pech-Canul, C. A. Gutiérrez, N. Soltani, Wetting and reaction characteristics of crystalline and amorphous SiO_2 derived rice-husk ash and SiO_2/SiC substrates with Al-Si-Mg alloys, Appl. Surf. Sci. 357 (2015) 1104–1113. doi:10.1016/j.apsusc.2015.09.137

[41] M. I. Pech-Canul, R. N. Katz, M. M. Makhlouf, Optimum conditions for pressureless infiltration of SiCp preforms by aluminum alloys, J. Mater. Process. Technol. 108 (2000) 68–77. doi:10.1016/S0924-0136(00)00664-6
[42] M. K. Aghajanian, M. A. Rocazella, J. T. Burke, S. D. Keck, The fabrication of metal matrix composites by a pressureless infiltration technique, J. Mater. Sci. 26 (1991) 447–454. doi:10.1007/bf00576541
[43] D. Xu, Z. Li, G. Wang, X. Li, X. Lv, Y. A. Zhang, Y. Fan, B. Xiong, Phase transformation and microstructure evolution of an ultra-high strength Al-Zn-Mg--Cu alloy during homogenization, Mater. Charact. 131 (2017) 285–297. doi:10.1016/j.matchar.2017.07.011
[44] K. Wen, B. Xiong, Y. Zhang, G. Wang, X. Li, Z. Li, S. Huang, H. Liu, Microstructure evolution of a high zinc containing Al-Zn-Mg-Cu alloy during homogenization, Rare Metal Mat. Eng. 46 (2017) 928–934. doi:10.1016/S1875-5372(17)30124-8
[45] B. D. Newsome, F. B. Schultz, B. J. Ferguson, K. P. Rohatgi, Synthesis and quasi-static compressive properties of Mg-AZ91D-Al_2O_3 syntactic foams, Materials 8 (2015) 6085–6095. doi:10.3390/ma8095292
[46] D. D. Luong, O. M. Strbik, V. H. Hammond, N. Gupta, K. Cho, Development of high performance lightweight aluminum alloy/SiC hollow sphere syntactic foams and compressive characterization at quasi-static and high strain rates, J. Alloys Compd. 550 (2013) 412–422. doi:10.1016/j.jallcom.2012.10.171
[47] C. A. Vogiatzis, A. Tsouknidas, D. T. Kountouras, S. Skolianos, Aluminum-ceramic cenospheres syntactic foams produced by powder metallurgy route, Mater. Des. 85 (2015) 444–454. doi:10.1016/j.matdes.2015.06.154
[48] X. F. Tao, L. P. Zhang, Y. Y. Zhao, Al matrix syntactic foam fabricated with bimodal ceramic microspheres, Mater. Des. 30 (2009) 2732–2736. doi:10.1016/j.matdes.2008.11.005
[49] G. H. Wu, Z. Y. Dou, D. L. Sun, L. T. Jiang, B. S. Ding, B. F. He, Compression behavior of cenosphere-pure aluminum syntactic foams, Scr. Mater. 56 (2007) 221–224. doi:10.1016/j.scriptamat.2006.10.008
[50] M. Taherishargh, I. V. Belova, G. E. Murch, T. Fiedler, Low-density expanded perlite-aluminium syntactic foam, Mater. Sci. Eng. A 604 (2014) 127–134. doi:10.1016/j.msea.2014.03.003
[51] A. Daoud, Compressive response and energy absorption of foamed A359-Al_2O_3 particle composites, J. Alloys Compd. 486 (2009) 597–605. doi:10.1016/j.jallcom.2009.07.013
[52] J. Zhang, Y. N. Huang, C. Mao, P. Peng, Structural, elastic and electronic properties of $\theta(Al_2Cu)$ and $S(Al_2CuMg)$ strengthening precipitates in Al-Cu-Mg series alloys: First-principles calculations, Solid State Commun. 152 (2012) 2100–2104. doi:10.1016/j.ssc.2012.09.003
[53] A. E. Markaki, T. W. Clyne, The effect of cell wall microstructure on the deformation and fracture of aluminium-based foams, Acta Mater. 49 (2001) 1677–1686. doi:10.1016/S1359-6454(01)00072-6
[54] T. Miyoshi, M. Itoh, T. Mukai, H. Kanahashi, H. Kohzu, S. Tanabe, K. Higashi, Enhancement of energy absorption in a closed-cell aluminum by the modification of cellular structures, Scr. Mater. 41 (1999) 1055–1060. doi:10.1016/S1359-6462(99)00255-9
[55] F. Han, Z. Zhu, J. Gao, Compressive deformation and energy absorbing characteristic of foamed aluminum, Metall. Mater. Trans. A 29 (1998) 2497–2502. doi:10.1007/s11661-998-0221-z
[56] A. Daoud, Synthesis and characterization of novel ZnAl22 syntactic foam composites via casting, Mater. Sci. Eng. A 488 (2008) 281–295. doi:10.1016/j.msea.2007.11.020
[57] A. D. Akinwekomi, J. A. Adebisi, A. A. Adediran, Compressive characteristics of aluminum-fly ash syntactic foams processed by microwave sintering, Metall. Mater. Trans. A 50 (2019) 4257–4260. doi:10.1007/s11661-019-05347-1
[58] S. Sahu, M. Z. Ansari, D. P. Mondal, C. Cho, Quasi--static compressive behaviour of aluminium cenosphere syntactic foams, Mater. Sci. Technol. 35 (2019) 856–864. doi:10.1080/02670836.2019.1593670
[59] S. Birla, D. P. Mondal, S. Das, N. Prasanth, A. K. Jha, A. N. C. Venkat, Compressive deformation behavior of highly porous AA2014-cenosphere closed cell hybrid foam prepared using CaH_2 as foaming agent: comparison with aluminum foam and syntactic foam, Trans. Indian Inst. Met. 70 (2017) 1827–1840. doi:10.1007/s12666-016-0984-7
[60] A. Wright, A. Kennedy, The processing and properties of syntactic Al foams containing low cost expanded glass particles, Adv. Eng. Mater. 19 (2017) 1600467. doi:10.1002/adem.201600467
[61] B. Zhang, Y. Lin, S. Li, W. Wang, G. Wu, Quasi-static and high strain rates compressive behavior of aluminum matrix syntactic foams, Composites, Part B 98 (2016) 288–269. doi:10.1016/j.compositesb.2016.05.034
[62] M. Taherishargh, M. Vesenjak, I. V. Belova, L. Krstulović-Opara, G. E. Murch, T. Fiedler, In situ manufacturing and mechanical properties of syntactic foam filled tubes, Mater. Des. 99 (2016) 356–368. doi:10.1016/j.matdes.2016.03.077
[63] J. A. Santa Maria, B. F. Schultz, J. B. Ferguson, N. Gupta, P. K. Rohatgi, Effect of hollow sphere size and size distribution on the quasi-static and high strain rate compressive properties of Al-A380-Al_2O_3 syntactic foams, J. Mater. Sci. 49 (2014) 1267–1278. doi:10.1007/s10853-013-7810-y
[64] S. Bazzaz Bonabi, J. Kahani Khabushan, R. Kahani, A. Honarbakhsh Raouf, Fabrication of metallic composite foam using ceramic porous spheres “Light Expanded Clay Aggregate” via casting process, Mater. Des. 64 (2014) 310–315. doi:10.1016/j.matdes.2014.07.061